Molecular Biology of the Cell
Vol. 10, 4075–4090, December 1999

Two Components of Actin-based Retrograde Flow in Sea Urchin Coelomocytes

John H. Henson,*†‡ Tatyana M. Svitkina,§ Andrew R. Burns,* Heather E. Hughes,* Kenneth J. MacPartland,* Ronniel Nazarian,*† and Gary G. Borisy§

*Department of Biology, Dickinson College, Carlisle, Pennsylvania 17013; †Mount Desert Island Biological Laboratory, Salisbury Cove, Maine 04672; and §Laboratory of Molecular Biology, University of Wisconsin, Madison, Wisconsin 53706

Submitted May 14, 1999; Accepted October 7, 1999
Monitoring Editor: Thomas D. Pollard

Sea urchin coelomocytes represent an excellent experimental model system for studying retrograde flow. Their extreme flatness allows for excellent microscopic visualization. Their discoid shape provides a radially symmetric geometry, which simplifies analysis of the flow pattern. Finally, the nonmotile nature of the cells allows for the retrograde flow to be analyzed in the absence of cell translocation. In this study we have begun an analysis of the retrograde flow mechanism by characterizing its kinetic and structural properties. The supramolecular organization of actin and myosin II was investigated using light and electron microscopic methods. Light microscopic immunolocalization was performed with anti-actin and anti-sea urchin egg myosin II antibodies, whereas transmission electron microscopy was performed on platinum replicas of critical point-dried and rotary-shadowed cytoskeletons. Coelomocytes contain a dense cortical actin network, which feeds into an extensive array of radial bundles in the interior. These actin bundles terminate in a perinuclear region, which contains a ring of myosin II bipolar minifilaments. Retrograde flow was arrested either by interfering with actin polymerization or by inhibiting myosin II function, but the pathway by which the flow was blocked was different for the two kinds of inhibitory treatments. Inhibition of actin polymerization with cytochalasin D caused the actin cytoskeleton to separate from the cell margin and undergo a finite retrograde retraction. In contrast, inhibition of myosin II function either with the wide-spectrum protein kinase inhibitor staurosporine or the myosin light chain kinase–specific inhibitor KT5926 stopped flow in the cell center, whereas normal retrograde flow continued at the cell periphery. These differential results suggest that the mechanism of retrograde flow has two, spatially segregated components. We propose a "push–pull" mechanism in which actin polymerization drives flow at the cell periphery, whereas myosin II provides the tension on the actin cytoskeleton necessary for flow in the cell interior.

INTRODUCTION

A wide variety of cells have been shown to exhibit the phenomenon of retrograde or centripetal flow in which there is a net transport of surface receptors and the underlying actin cytoskeleton from the cell edge toward the cell center (Bray and White, 1988; for recent reviews, see Mitchison and Cramer, 1996; Mogilner and Oster, 1996; Heidemann and Buxbaum, 1998). This process has been studied most extensively in motile cells, including neuronal growth cones (Forscher and Smith, 1988; Mitchison and Kirschner, 1988; Smith, 1988; Lin and Forscher, 1995; Suter *et al.*, 1998), cultured fibroblasts and epithelial cells (Heath, 1983; Wang, 1985; Debasio *et al.*, 1988; Fisher *et al.*, 1988; Verkhovsky *et al.*, 1995; Cramer *et al.*, 1997; Waterman-Storer and Salmon, 1997), and fish keratocytes (Theriot and Mitchison, 1991; Lee *et al.*, 1993; Svitkina *et al.*, 1997). In freely moving keratocytes, the retrograde flow is relative to the leading edge, because both actin and myosin II are stationary with respect to the substrate (Theriot and Mitchison, 1991; Svitkina *et al.*, 1997).

Although a multiplicity of models for retrograde flow have been proposed (Cramer, 1997), the simplest mechanism is that retrograde flow is a necessary consequence of contractile force between the lamellipodium and the cell body (Verkhovsky *et al.*, 1999). In this view, contractile forces

‡ Corresponding author. E-mail address: henson@dickinson.edu.

drive the cell body forward when the lamellipodium is more firmly attached to the substratum than the cell body. However, should the cell body be tethered or more firmly adherent than the lamellipodium, retrograde flow of lamellipodial structures will result. An essential feature of this viewpoint is that the retrograde flow is balanced by polymerization of actin and assembly of the contractile machinery at the leading edge. Evidence consistent with this viewpoint comes from a number of studies. In fibroblasts, several lines of investigation have suggested the importance of actin polymerization in lamellipodial centripetal flow (Wang, 1985, 1987), and that transversely oriented actin and myosin II structures found at the bases of lamellipodia may be contributing to the centripetal flow process (Debasio *et al.*, 1988: Conrad *et al.*, 1989, 1993; Verkhovsky *et al.*, 1995). One of the best studied model systems for retrograde flow is the *Aplysia* bag neuron growth cone, in which Forscher and coworkers have conducted a number of critical studies on actin structure and dynamics and the possible involvement of myosin motors (Forscher and Smith, 1988; Forscher *et al.*, 1992; Lin and Forscher, 1993, 1995; Lin *et al.*, 1996). They have argued for a role for myosins in driving actin-based retrograde flow, because injection of myosin S-1 and treatment with the putative low affinity actomyosin inhibitor 2,3-butanedione monoxime (BDM) both stopped retrograde movement (Lin *et al.*, 1996). In keratocytes, recent studies have indicated the importance of actin polymerization at the edge and myosin II contraction forces in the lamellipodial–cell body transition region in the mediation of locomotion in moving cells (Anderson *et al.*, 1996; Svitkina *et al.*, 1997). Thus, the exisiting literature provides a number of example systems implicating the acto-myosin II machinery in retrograde flow. However, in no case is the mechanism definitively established. Impediments in analyzing retrograde flow have been the slowness of the process and the spatial complexity of the cytoskeleton. With these problems in mind, we have sought a more favorable system in which to investigate the phenomenon.

Sea urchin coelomocytes represent an excellent and unique alternative experimental model system for the study of actin-based retrograde flow. Once settled onto a substrate, one subtype of these cells forms exceedingly flat and stationary discs and engages in rapid retrograde and centripetal flow, originating along the entire perimeter of the cell (Edds, 1993a). In this study, we have focused on attempting to elucidate the role of myosin II in coelomocyte centripetal flow. Despite the major advances made in research on unconventional myosins (for reviews, see Mooseker and Cheney, 1995; Ostap and Pollard, 1996), conventional myosin II remains the only myosin type capable of forming bipolar minifilaments, which can interact with actin in a contractile manner (Cheney *et al.*, 1993), and myosin II knockout experiments in *Dictyostelium* have demonstrated its involvement in cell locomotion (Jay *et al.*, 1995). In our experiments, we used light microscopic immunocytochemical localization in conjunction with critical point drying and rotary replication transmission electron microscopy (TEM) methods to examine the actin and myosin II filament structure in coelomocytes undergoing centripetal flow. The results of these studies demonstrate the arrangement of actomyosin structures both in control cells and in cells in which the centripetal flow process has been arrested or altered. In untreated cells, actin filaments at the periphery feed into radial bundles that connect with a unique array of myosin bipolar filaments in the cell center. This spatial segregation of the actin-myosin II machinery simplifies analysis of its role in retrograde flow. Drug-based function-blocking experiments were also conducted, and these clearly indicate that the flow mechanisms operating at the cell periphery are distinct and can be uncoupled from those operating in the cell interior. Taken together, these structural and drug-based studies argue for a two-component model for retrograde flow in which actin polymerization drives flow at the cell periphery, whereas myosin II provides the tension on the actin cytoskeleton necessary for flow in the cell interior.

MATERIALS AND METHODS

Animals, Cell Preparation, and Reagents

Sea urchins of the species *Strongylocentrotus droebachiensis* were collected from the near-shore waters surrounding the Mount Desert Island Biological Laboratory in Maine and kept in either running sea water or closed artificial sea water systems at 15°C. Coelomocytes were isolated and maintained as described by Henson *et al.* (1992) with the coelomocyte culture media (CCM) consisting of 0.5 M NaCl, 5 mM $MgCl_2$, 1 mM EGTA, and 20 mM HEPES, pH 7.2. Typically the cells were used within 2–8 h of isolation. An anti-sea urchin egg myosin II heavy chain antiserum was generated by immunizing rabbits with electrophoretically purified myosin II heavy chain, which had been ATP precipitated as filaments from high-speed supernatants of *S. purpuratus* egg extracts using the methods of Bryan and Kane (1982). A monoclonal anti-actin antibody (clone C4) was obtained from ICN (Costa Mesa, CA); rhodamine-phalloidin was purchased from Molecular Probes (Eugene, OR); KT5926 came from Calbiochem (Costa Mesa, CA); and the majority of other reagents and antibodies were purchased from Sigma (St. Louis, MO).

Digitally Enhanced Video Microscopy and Retrograde Flow Measurements

Coelomocytes were settled onto either untreated or 0.1 mg/ml poly-L-lysine–coated glass coverslips, which were then mounted in perfusion chambers constructed of coverslip shims placed on a slide. Cells were viewed on a Nikon (Tokyo, Japan) Optiphot 2 microscope using a 60× (numerical aperture, 1.4) plan-apo phase-contrast objective lens. Video images were obtained with a Dage (Michigan City, IN) MTI 70S Newvicon camera coupled to a Hamamatsu (Hamamatsu City, Japan) Argus-10 real-time digital image processor. Frame-averaged, background-subtracted, and contrast-enhanced images were recorded on a Javelin (Torrance, CA) JR4500 time-lapse VCR, and still images were printed using a Mitsubishi (Tokyo, Japan) P40U video copy processor. Time-lapse recordings were typically done in the range of 6- to 12-fold time compression.

Measurements of the rate of retrograde flow in cells were accomplished by tracking the inward movements of phase-light arcs (corresponding to areas of low actin filament concentration; see Figure 3) and/or phase-dense membranous structures in the cells. Flow measurements were possible over a range of 70–80% of the radius of the cell, with flow in the cell center obscured by the phase halo of the nuclear region. In some experiments the movement of latex beads settled onto the surface of cells was measured; however, this was done with the caveat that some of the beads exhibited independent (often anterograde) motility, similar to that seen with growth cones ("inductopodia" in Forsher *et al.*, 1992). The differences between the means of flow rates in cells under different experimental conditions were tested for statistical significance using a two-tailed *t* test with the $p = 0.01$.

Immunoblotting

For Western immunoblotting, gel samples of high-speed supernatants of sea urchin eggs and coelomocytes were run on 4% SDS-polyacrylamide gels and then transferred onto nitrocellulose. The nitrocellulose filters were blocked with 5% nonfat dry milk in Tris-buffered saline and incubated in 1:3000 dilution of the anti-sea urchin myosin, followed by incubation in the alkaline phosphatase-conjugated goat anti-rabbit immunoglobulin G secondary antibody.

Fluorescent Localization

For either rhodamine-phalloidin staining alone or for double labeling for tubulin, cells were fixed in 0.25% glutaraldehyde plus 0.5% Triton X-100 in buffer A (75 mM KCl, 2 mM $MgCl_2$, 320 mM sucrose, 20 mM EGTA, and 20 mM 1,4-piperazinediethanesulfonic acid, pH 7.0) for 10 min. For immunofluorescence staining of actin and myosin, cells were prefixed in 0.001% glutaraldehyde in CCM for 5 min (after Hyatt *et al.*, 1984), fixed in 1% formaldehyde and 0.5% Triton X-100 in buffer A for 10 min, and then postfixed in 100% methanol at −20°C for 10 min. After a rinse with PBS, cells were blocked with PBS plus 1% BSA and 2% goat serum and stained with primary antibodies followed by the appropriate fluorescently labeled secondary antibodies. Cells were mounted in anti-photobleach and viewed using a 60× (numerical aperture, 1.4) plan-apo phase-contrast objective lens, and 35-mm micrographs were taken using Kodak TriX 400 film (Eastman Kodak, Rochester, NY).

Critical Point-drying and Rotary-shadowing TEM

Transmission electron microscopic imaging of critical point-dried and rotary-shadowed replicas of coelomocyte cytoskeletons followed methods described previously for fibroblasts and keratocytes (Svitkina *et al.*, 1989, 1995, 1997). Briefly, coelomocytes were either prefixed in 0.001% glutaraldehyde in CCM or left unfixed and then extracted in 0.5% Triton X-100 in buffer A, buffer B (100 mM NaCl, 5 mM $MgCl_2$, 10 mM EGTA, and 20 mM HEPES, pH 7.O), or buffer C (polyethylene glycol-supplemented extraction buffer; described by Svitkina *et al.*, 1995). For actin depletion, detergent-extracted cytoskeletons were treated with 0.1–0.2 mg/ml gelsolin for 30 min. After extraction, the cells were then fixed in 2.5% glutaraldehyde in the same buffer. Then the cells were dehydrated in graded ethanols, critical point dried, and rotary shadowed with platinum and carbon. Metal replicas were separated from glass coverslips using hydrofluoric acid, mounted on Formvar-coated grids, and observed and photographed on either a Phillips (Eindhoven, The Netherlands) 300 or a Zeiss (Thornwood, NY) EM-109 transmission electron microscope, operating at 60–80 kV.

Pharmacological Treatments for Disrupting Retrograde Flow

Coelomocyte retrograde flow was disrupted by treatment with one of the following drugs diluted into CCM: 1 μM cytochalasin D, 0.5–3 μM staurosporine, 250–500 nM KT5926, or 15 mM BDM. All of the drugs except BDM were diluted from stock solutions dissolved in DMSO, and in these cases the appropriate DMSO-alone controls were performed.

RESULTS

Coelomocyte Subtypes, Immunoblotting, and Light Microscopic Localization of Actin and Myosin II

Past studies have established that sea urchin coelomocytes, as conventionally isolated, consist of at least two distinct subtypes (Henson *et al.*, 1992; Edds, 1993a,b). Subtype 1 cells are discoid shaped and stationary, have a radially arranged actin cytoskeleton and a limited perinuclear microtubule array, and undergo rapid centripetal flow throughout the bulk of the cell's cytoplasm. The rate of centripetal flow in these cells ranges between 2 and 5 μm/min. Subtype 2 cells are polygonal in shape and motile, have a dense actin cytoskeleton complete with stress fiber-like structures and a widespread microtubule array, and undergo slower centripetal flow with characteristic ruffling at the margins of the cell. In many ways the subtype 1 cells are analogous to a 360° growth cone, whereas the subtype 2 cells are more like cultured fibroblasts. In the present study we have concentrated on the rapid and regular centripetal flow displayed by subtype 1 cells; however, we also took advantage of the opportunity to compare structural features between the two cell types whenever possible.

Video-enhanced microscopy showed the radial nature of cytoplasmic organization in the discoidal subtype 1 cells and clearly revealed the occurrence of centripetal flow (Figure 1). In many cells the inward flow of the cytoskeleton could be tracked by examining the position of either phase-dense small membranous elements or white arcs that appeared in the cytoplasm (Figure 1, arrows). These arcs moved persistently and at uniform velocity toward the cell center. As will be shown in the next section, the white arcs corresponded to regions of lower actin filament concentration. Measurements of flow rates in control cells indicated a mean of 3.7 μm/min (SD = 1.6 μm/min, as shown in Figure 9), with the rate remaining constant over the ~75% of the cell radius available for measurement.

To establish the distribution of actin and myosin in coelomocytes, we initially performed light microscopic immunolocalization using anti-actin and anti-sea urchin myosin II antibodies. Immunoblotting of the anti-sea urchin myosin II heavy chain antiserum against the high-speed supernatant of lysates from eggs and coelomocytes (run on low-percentage gels) demonstrated the monospecificity of this antiserum (Figure 2) and suggested, perhaps not surprisingly, that coelomocytes may express a different myosin II heavy chain isoform than that present in eggs. Anti-actin staining of subtype 1 coelomocytes (Figure 3, A and B) showed the presence of an outer dense network of actin filaments and an array of inner radial bundles terminating in a perinuclear ring-like structure. Dark arcs in the anti-actin staining patterns (Figure 3C) corresponded to the white arcs seen by video microscopy, confirming that the white arcs are regions of lower actin concentration. Anti-myosin labeling (Figure 3, B and D) indicated that myosin distribution was restricted to the perinuclear region, where it formed a stellate, circular structure. Thus, the subtype 1 coelomocyte displayed a unique spatial segregation of the two major components of the contractile machinery. Actin filaments are distributed throughout the cytoplasm, whereas myosin II is restricted to the cell center.

The unusual distribution of myosin II in subtype 1 coelomocytes prompted us to carry out further tests of the reactivity of the myosin antibody in different cell types. In dividing sea urchin embryos, the myosin antibody stained the cleavage furrow as expected (our unpublished data). In the fibroblast-like, subtype 2 coelomocyte, myosin staining was distributed throughout the cytoplasm, often aligning with actin filament bundles in a stress fiber-like pattern as expected (Figure 3, E and F). Thus, the myosin antibody specifically labeled structures in sea urchin cells known to con-

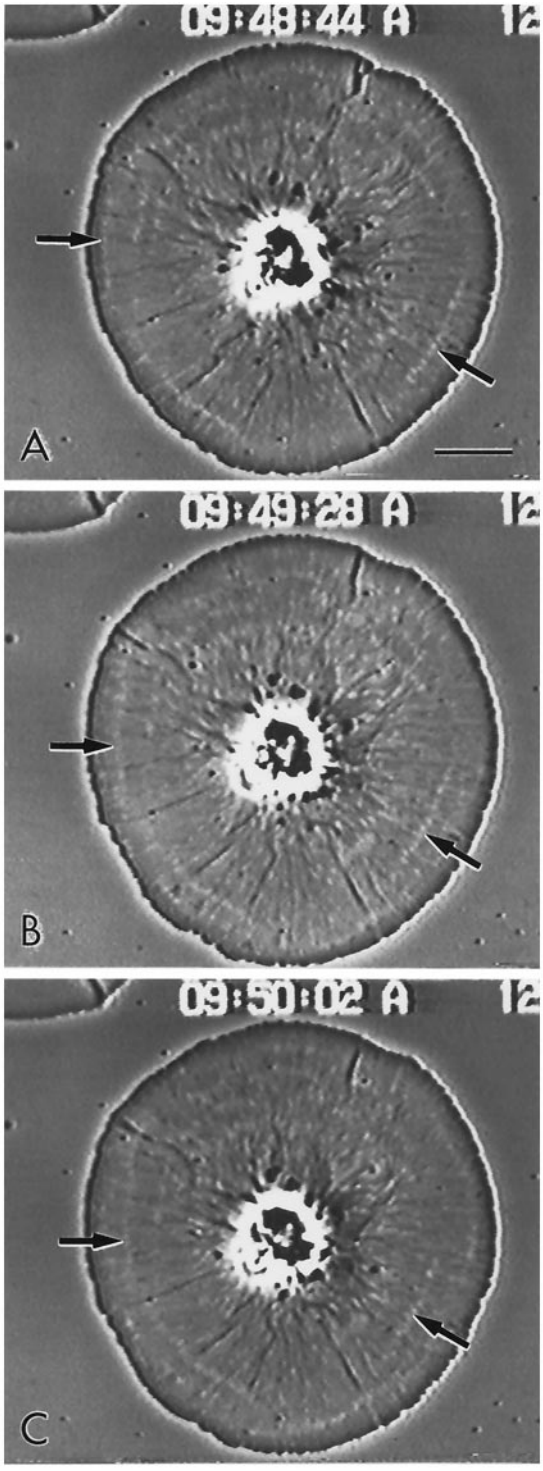

Figure 1. Video-enhanced phase contrast microscopy of living subtype 1 cell showing the radial nature of the actin cytoskeleton in a cell undergoing retrograde flow. The inward flow of the membrane and the underlying actin cytoskeleton can be tracked by following the movement of white arcs in the cytoplasm (arrows). These arcs represent discontinuities in the actin cytoskeleton (see Figure 3C). Bar, 10 μm.

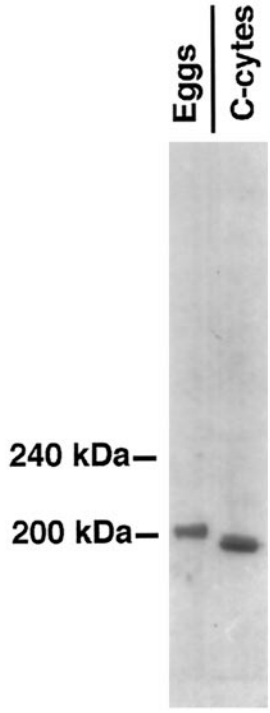

Figure 2. Immunoblot of anti-sea urchin egg myosin II heavy chain against high-speed supernatant samples from sea urchin eggs and coelomocytes (C-cytes) run on 4% gels. The antiserum monospecifically labels a band of ~200 kDa in the egg sample lane and a band of slightly lower molecular mass in the coelomocyte lane.

tain myosin. We infer that the myosin staining seen in subtype 1 coelomocytes is specific and represents a unique, central myosin structure. Note that double labeling of the two coelomocyte subtypes for actin filaments and microtubules (Figure 4) demonstrates the limited, perinuclear microtubule distribution present in subtype 1 cells (Figure 4, upper left cell) and the widely spread, extensive array of microtubules present in subtype 2 cells (Figure 4, lower right cell).

Supramolecular Organization of Actin and Myosin II

The supramolecular organization of the coelomocyte cytoskeleton was visualized by electron microscopy of platinum replicas. This type of imaging revealed that the discoid-shaped subtype 1 coelomocytes contained two distinct zones of actin cytoskeletal organization (Figure 5). The outer zone consisted of a dense brush-like network of actin filaments, which displayed free filament ends at the perimeter and a multilayered array of diagonally oriented filaments similar to that reported for keratocytes (Svitkina *et al.*, 1997; Figure 5C). A small subpopulation of long filaments in this zone were oriented tangentially with respect to the edge of the cell and the direction of centripetal flow (Figure 5C). Interior to the peripheral brush-like zone, the actin filament density was lower, and the filaments were organized both in loose networks and radially arrayed bundles (Figure 5D). Many

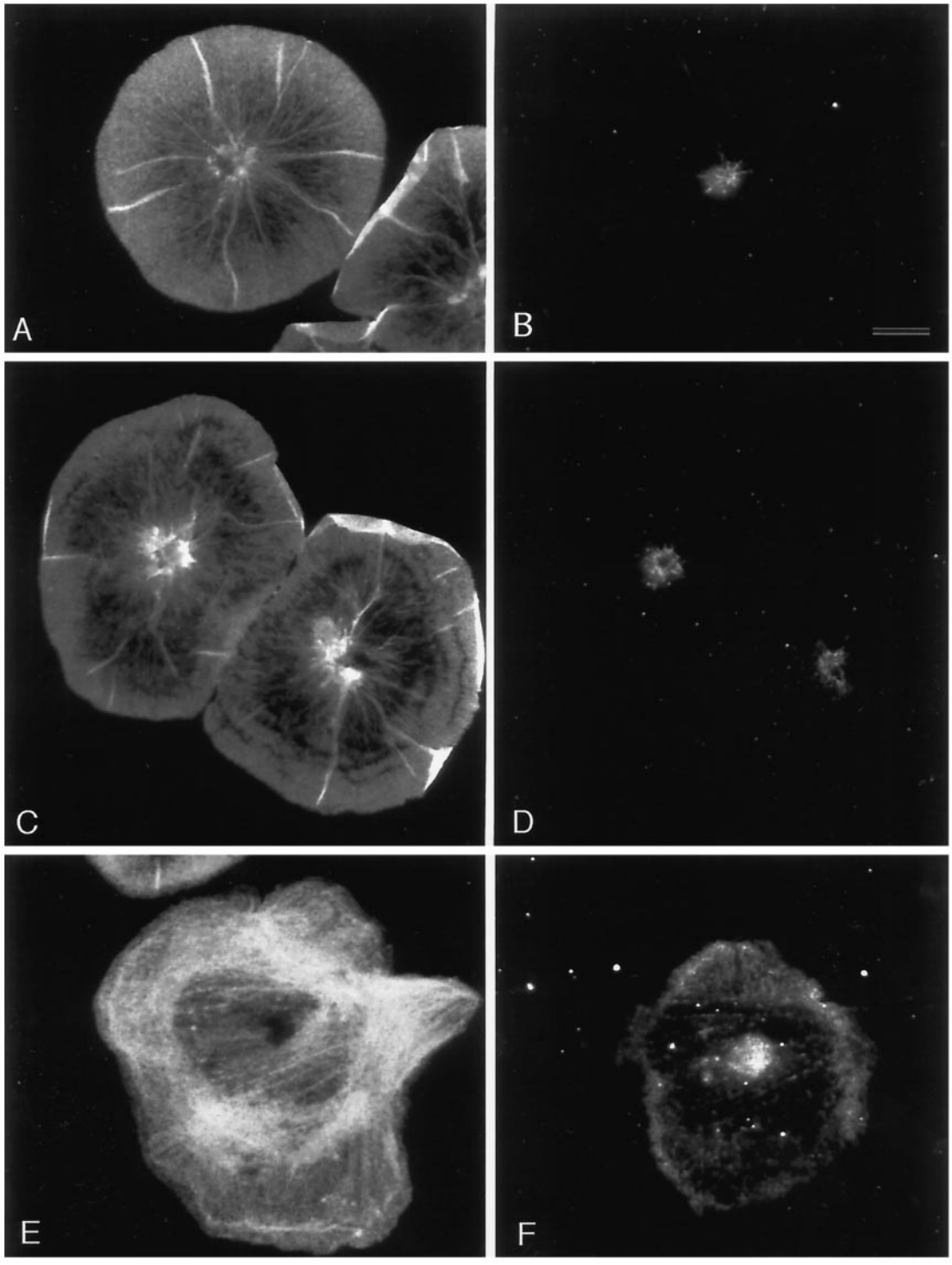

Figure 3. Immunolocalization of actin (A and C) and myosin II (B and D) in subtype 1 cells shows actin filaments arrayed in a dense cortical network, which feeds into inner radial bundles, as well as the perinuclear distribution and ring-like nature of the myosin staining pattern. Note that the dark arcs in the actin staining pattern (C) correspond to the white arcs present in video-enhanced images of living cells (Figure 1) and represent areas of low actin filament concentration. Immunolocalization of actin (E) and myosin II (F) in a subtype 2 cell shows that, in contrast to the perinuclear myosin ring present in subtype 1 cells, myosin in subtype 2 cells is widely distributed in the cytoplasm and often aligns itself with transverse stress fiber-like actin bundles. Bar, 10 μm.

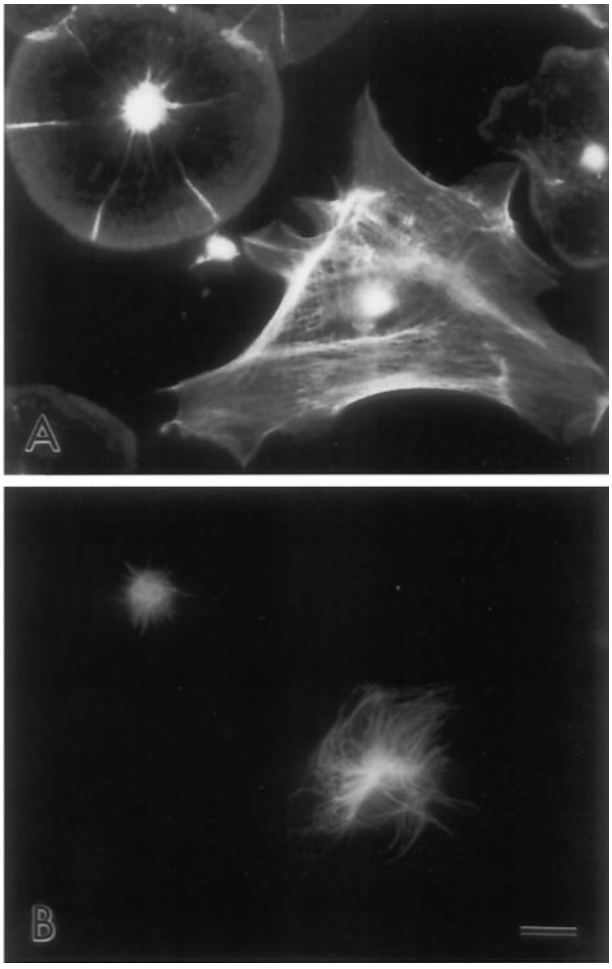

Figure 4. Immunofluorescent labeling of actin (A) and tubulin (B) in coelomocyte subtypes shows a limited, perinuclear microtubule array in subtype 1 cells (upper left cell), whereas subtype 2 cells (lower right cell) display a widespread microtubule array. Bar, 10 μm.

filaments within this zone appeared very long and could be traced for tens of micrometers. Some of the actin bundles at their distal terminus penetrated into and retained their integrity within the peripheral meshwork. At their proximal terminus, these bundles entered a dense perinuclear central structure. Light and electron microscopy indicated that this innermost zone was complex, containing microtubules and the remnants of organelles, including the nucleus. Overall, the electron microscopic view of the coelomocyte cytoskeleton agreed well with the conclusions drawn from both the video-enhanced microscopy of living cells and the immunofluorescence microscopy of fixed cells.

The abundance of actin filaments in the coelomocyte cytoskeleton precluded direct visualization of minor components. Following a strategy adopted previously in studies on fibroblasts (Verkhovsky *et al.*, 1995) and keratocytes (Svitkina *et al.*, 1997), actin filaments were removed by treatment with the actin-severing protein gelsolin (see MATERIALS AND METHODS). The gelsolin treatment allowed for the visualization of non-actin, detergent-insoluble cytoskeletal elements. Electron microscopic imaging of replicas from gelsolin-extracted subtype 1 cells revealed a perinuclear ring of short filaments (Figure 6A). At higher magnification (Figure 6, B and C), these filaments were resolved as bipolar filaments with morphology and dimensions similar to that previously established for myosin II. Their dumbbell appearance (smooth rod-like middle zone with globular heads at either end), average length (0.35–0.4 μm) and arrangement in head-to-head polygonal networks and side-to-side clusters are all features identical to those seen with myosin bipolar filaments in fibroblasts (Verkhovsky and Borisy, 1993) and keratocytes (Svitkina *et al.*, 1997). The strong correlation between the perinuclear ultrastructural distribution of these filaments and the light microscopic myosin immunolocalization data (Figure 3, B and D) also supports the conclusion that these filaments contain myosin II. Thus, subtype 1 coelomocytes display a unique distribution of myosin II, in which it is absent throughout the cytoplasm except for a central network of bipolar filaments. Note that the identification of the gelsolin-extracted cells in Figure 6 as subtype 1 is substantiated by the distribution of microtubules. The majority of microtubules (Figure 6, A and B, large, curved filaments) are restricted to the perinuclear region of these cells, a pattern shown by subtype 1 cells immunofluorescently labeled for tubulin (Figure 4).

Electron microscopy of cytoskeletons from gelsolin-extracted subtype 2 coelomocytes showed that myosin bipolar filaments were widely distributed in the cytoplasm of these fibroblast-like cells (our unpublished data), as would be expected from the anti-myosin immunofluorescence (Figure 3F) and similar to the distribution of myosin II filaments reported in fibroblasts (Verkhovsky and Borisy, 1993). The appearance of extensive myosin bipolar filament arrays in the subtype 2 cells argues against the possibility that the unique perinuclear distribution seen in subtype 1 cells is an artifact generated from the selective extraction of myosin from nonperinuclear regions. In addition, we see no evidence for the selective loss of actin filaments from the front of the lamellipodia of subtype 1 cells, a result reported by Small *et al.* (1995) in studies involving whole-mount negative stain TEM of fish keratocytes. They suggested that prefixation extraction led to the abolishment of a filament density gradient in these cells. However, we see a clear gradient in actin filament density at both the light microscopic (Figure 3) and TEM levels (Figure 5), and we also notice little difference between the cytoskeletons of cells detergent extracted either before or after fixation.

Disruption of Centripetal Flow

The spatial segregation of actin and myosin II in the subtype 1 coelomocytes suggested the possibility of distinguishing between mechanisms of retrograde flow by examining the consequences of inhibitory agents on the structural pattern. A range of agents was used to inhibit actin polymerization and myosin II function. We used cytochalasin D treatment as a means for determining the effect of lowered actin polymerization rates on coelomocyte centripetal flow. In cells exposed to cytochalasin D, the internal cytoskeleton continued to flow inward for a finite (~5-min) period, whereas a fringe region developed at the periphery (Figure 7, A–C). This fringe region was devoid of actin, except for a very thin

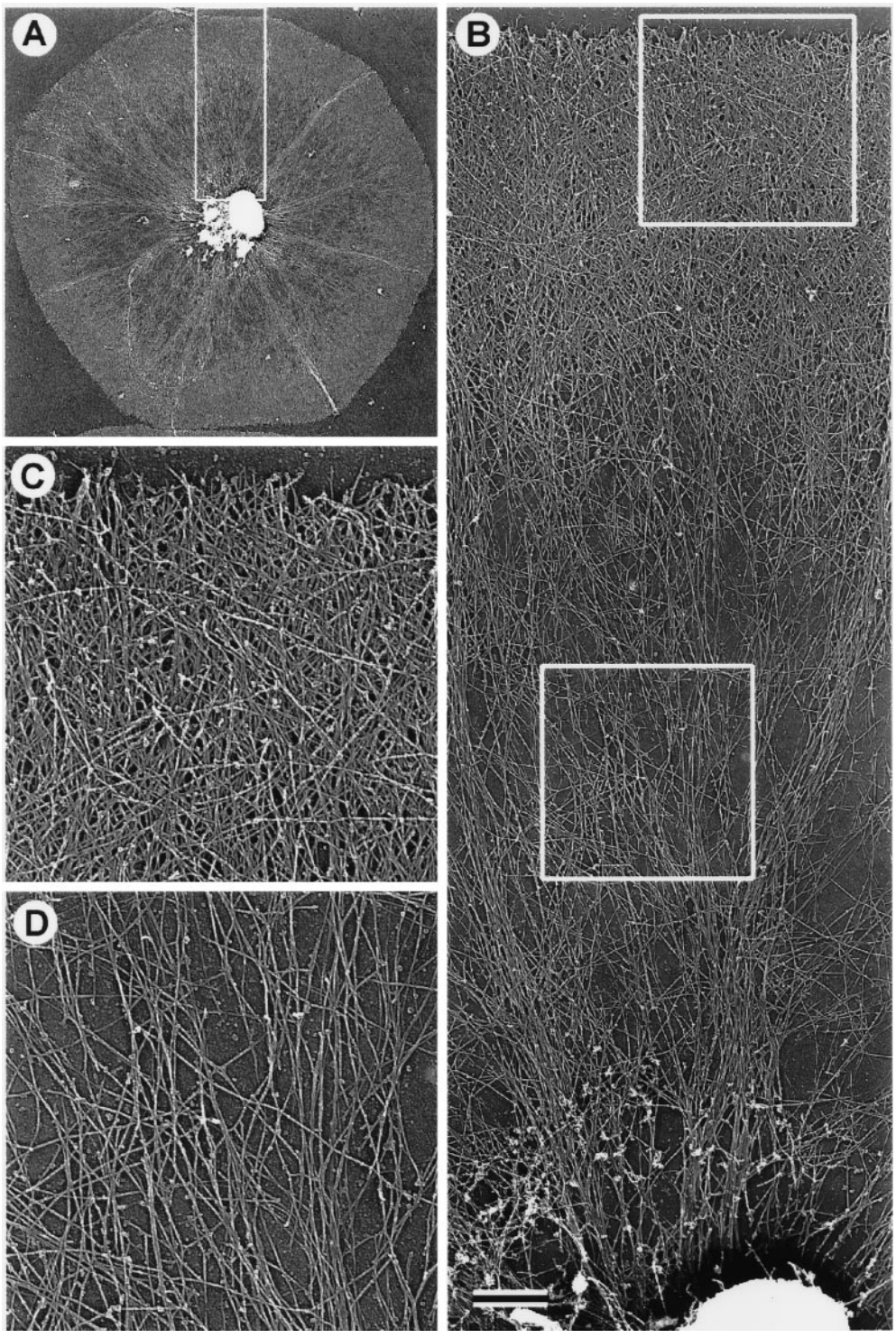

Figure 5. TEM of a critical point-dried and rotary-shadowed cytoskeleton from a subtype 1 coelomocyte. (A) Low-magnification view of a coelomocyte cytoskeleton. The box in A outlines the region that appears magnified in B, whereas the boxes in B outline the regions shown at higher magnification in C (upper box) and D (lower box). The outer cortical region of the cell consists of a dense meshwork of diagonally oriented actin filaments (B and C) containing a subset of elongated filaments oriented tangential to the edge of the cell (C). Inward from the cortical meshwork the actin organization changes to one containing radial bundles and loose actin arrays (B and D). Note the apparent continuity within the actin cytoskeleton throughout the cell and the fact that individual actin filaments can be traced for long distances. The complex perinuclear region containing actin filament terminations, microtubules, and the remnants of organelles appears at the bottom of B. Bar, 1 μm.

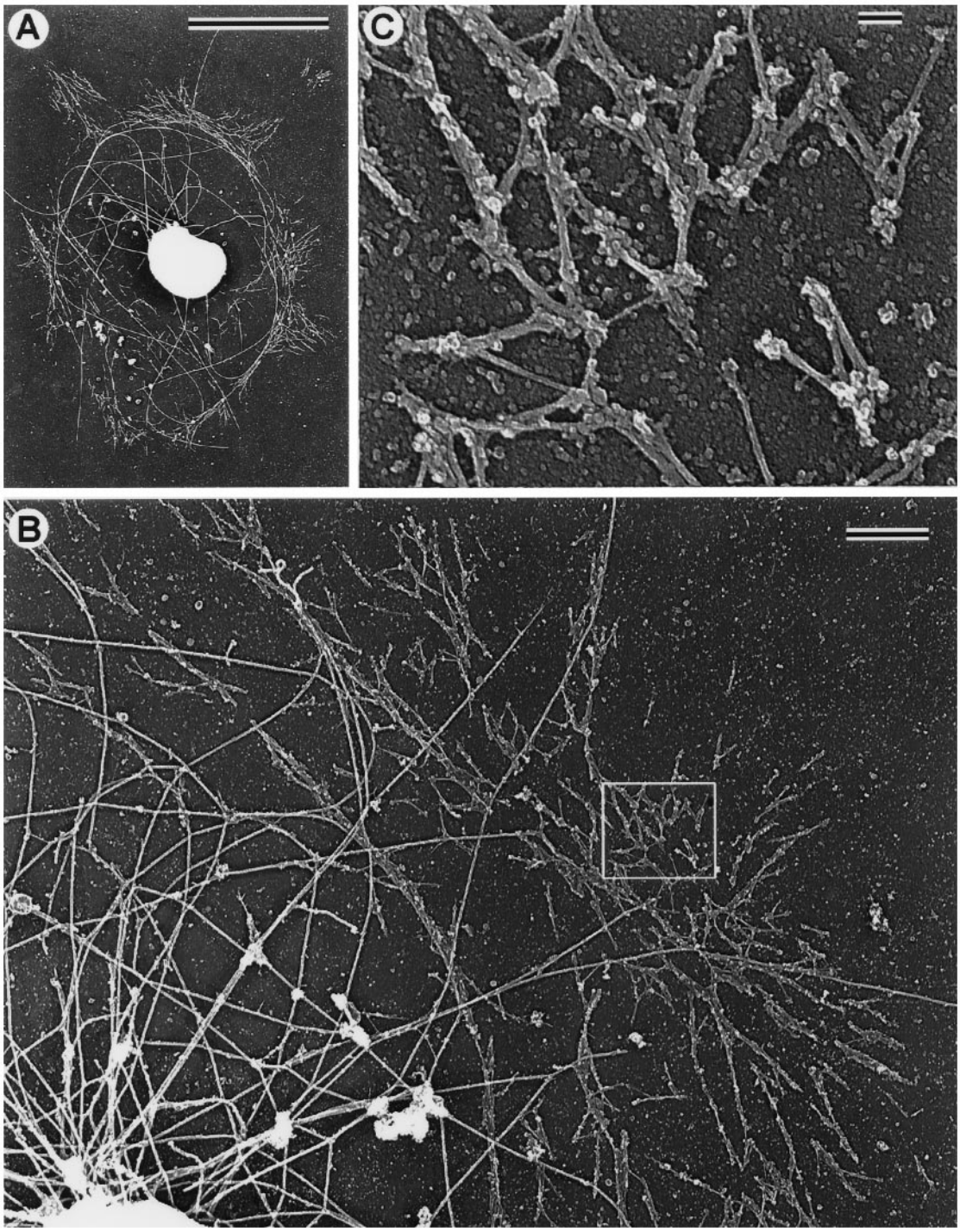

Figure 6. TEM of critical point-dried and rotary-shadowed cytoskeletons from gelsolin-extracted subtype 1 coelomocytes. (A) Low-magnification view of an extracted cytoskeleton revealing the presence of distinct short myosin bipolar filaments arrayed in a ring around the nucleus of the cell. Note that the myosin filaments form pyramidal-shaped aggregates, which extend away from the nucleus. (B) Higher-magnification view of a perinuclear ring of myosin filaments, with the box outlining a region at even higher magnification in C. These images indicate that the filamens are clearly myosin-like in their appearance (dumbbell shape with naked rod and globular heads) and organization (head-to-head and side-to-side associations as well as networks). Note that microtubules (large, curved filaments) are largely restricted to the region inside of the myosin ring in these cells. Bars: A, 10 μm; B, 1 μm; C, 0.1 μm.

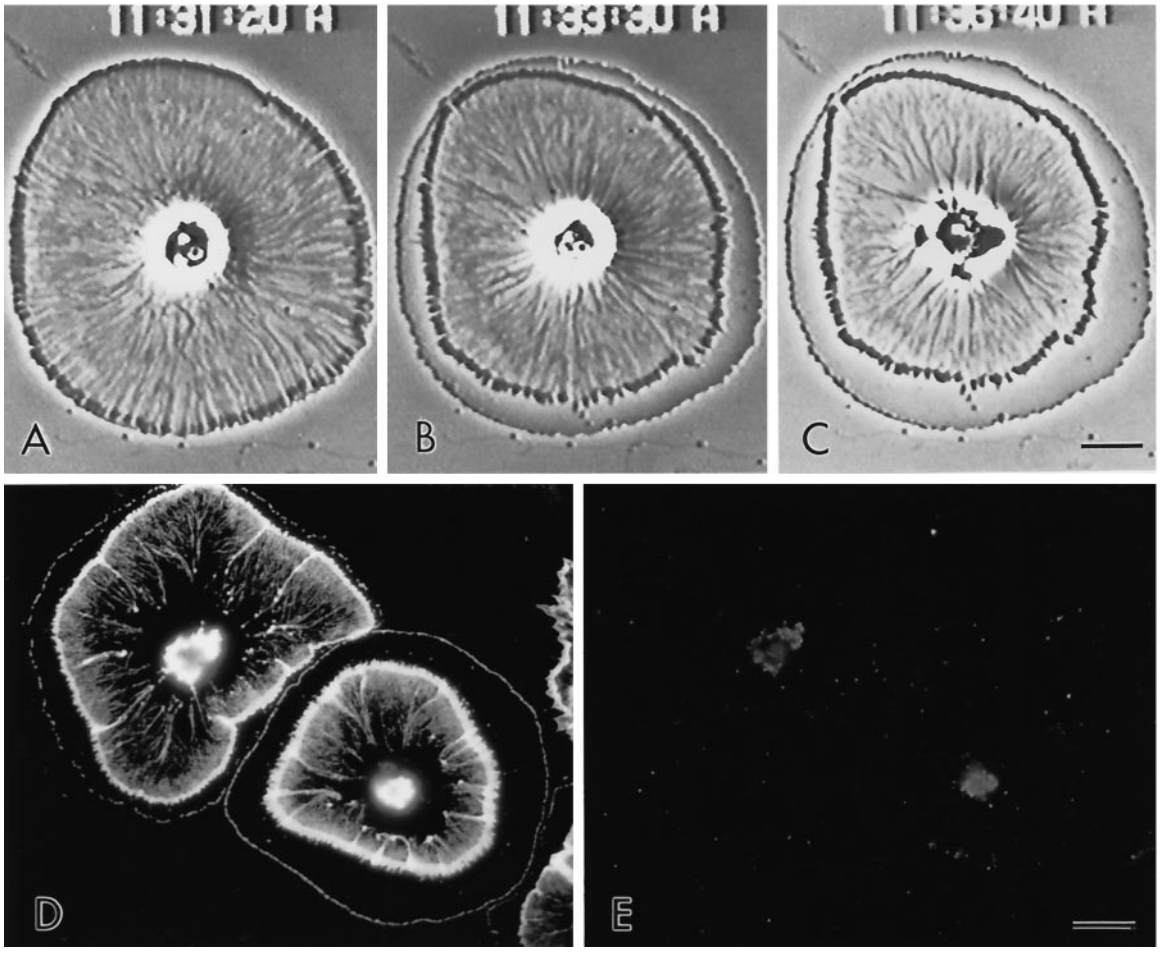

Figure 7. (A–C) Video-enhanced microscopy of subtype 1 coelomocyte treated with 1 μM cytochalasin D. The treatment (started at 11:30:30) stops peripheral flow and causes the development of a cortical actin-free fringe as the central cytoskeleton exhibits a finite retraction away from the cell edge. After several minutes in cytochalasin (C), the central actin cytoskeleton becomes disrupted. (D and E) Actin (D) and myosin II (E) immunolabeling of coelomocytes exposed to cytochalasin for 10 min. Note that the cortical fringe is devoid of actin and that the central cytoskeleton is greatly disrupted. Bar, 10 μm.

actin-containing zone at the original position of the cell margin (Figure 7D), and the width of the fringe varied within the range of 10–40% of the cell radius. A similar cytochalasin D-induced fringe has been previously reported in coelomocytes (Edds, 1993a), and in growth cones (Forscher and Smith, 1988). Interpretation of this actin-free fringe is that it is created by the continued retraction of the cytoskeleton toward the cell center, whereas polymerization of actin at the periphery is blocked. Therefore, these results indicate the existence of a component of the flow mechanism not dependent on actin polymerization. In growth cones, this retraction response has been used as evidence for the existence of a myosin-mediated contractile tension exerted on the peripheral cytoskeleton (Forscher and Smith, 1988). Prolonged cytochalasin exposure in the coelomocytes resulted in the dissolution of the central actomyosin cytoskeleton, as evidenced by video-enhanced microscopy of living cells (Figure 7C) and by actin and myosin labeling of fixed cells (Figure 7, D and E).

Myosin function was inhibited by use of the broad protein kinase inhibitor staurosporine (1–3 μM) and the more myosin light chain kinase-specific inhibitor KT5926 (250–500 nM) (Nakanishi *et al.*, 1990; Kazuo *et al.*, 1998). Treatment of coelomocytes with either inhibitor resulted in a similar response (Figure 8) in which flow continued in the peripheral region but was halted within the cell interior. The width of the peripheral region exhibiting persistent flow varied within the range of 20–40% of the cell radius. This resulted in the development of a medial ridge of accumulated membrane and cytoskeletal material at the interface between the periphery and the interior together with the disruption of the radial pattern of actin organization, as evidenced by video-enhanced microscopy of live cells (Figure 8, A and B) and fluorescence staining of actin in fixed cells (Figure 8, D and E). Double labeling for actin and myosin II indicated that the kinase inhibitors also disrupted the organization of the perinuclear myosin ring (Figure 8F). It is significant to note that the actin organization at the periphery of the

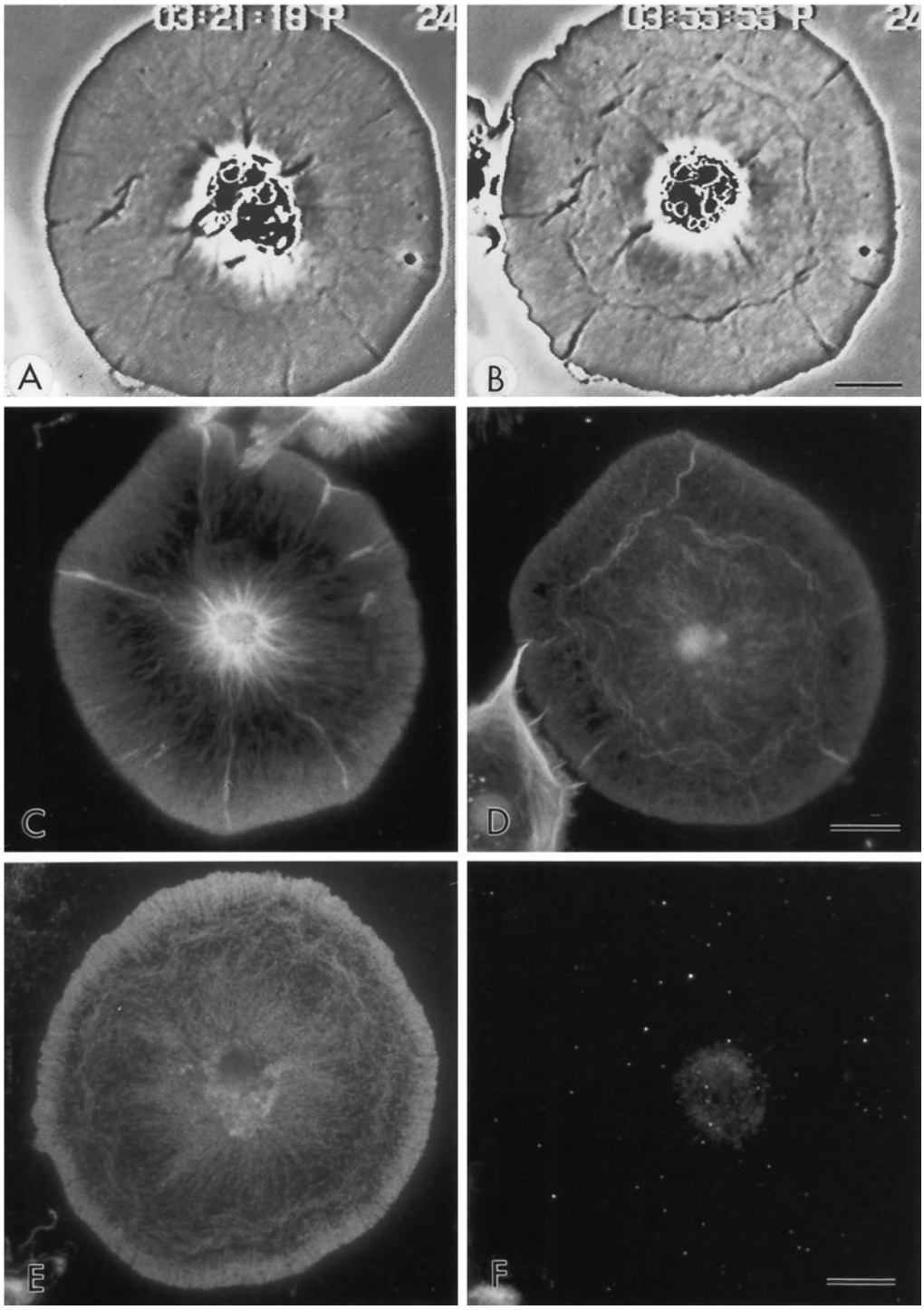

Figure 8. Video-enhanced microscopy of a control subtype 1 coelomocyte (A) and the same cell after exposure to 2 μM staurosporine for 15 min (B). The treatment results in the stoppage of flow in the cell center and the continuance of flow in the cell periphery. This results in the buildup of a notable medial ridge of cytoskeletal and membrane material in between the cortex and the cell center. Rhodamine-phalloidin staining of control (C) and staurosporine treated (D) cells shows that the structural organization of actin in the cell cortex is quite similar; however, there is clearly a disruption of the central actin radial array under the influence of the kinase inhibitor. In addition, the accumulation of actin is seen in the inhibitor-induced medial ridge. Actin (E) and myosin (F) labeling of a cell treated with 500 nM KT5926 shows an actin arrangement similar to that seen with staurosporine (D) and also demonstrates that the perinuclear myosin ring has become disorganized coincident with the rearrangement of the central actin cytoskeleton and the arrest of interior flow. Bar, 10 μm.

inhibitor-treated cells, which retains retrograde flow, appears very similar to controls. These results suggest that myosin II function is needed for retrograde flow in the interior but not at the periphery and indicate the existence of a component of the flow mechanism independent of myosin II function.

If two separable components of retrograde flow exist, inhibitable by different reagents, then combined or sequential application of both types of reagent should completely inhibit flow. Subtype 1 coelomocytes were treated with either of the protein kinase inhibitors and then treated with cytochalasin D. Under these conditions, the peripheral clear fringe that appears in cells treated only with cytochalasin D failed to appear. Thus, the effects of the two types of inhibitors were additive. The results support the notion that the cytochalasin-induced fringe is a result of myosin-dependent contractile tension on the central cytoskeleton and that the kinase inhibitors interfere with this tension.

The quantitation of retrograde flow rates in control and inhibitor-treated cells was carried out to determine whether there were any significant differences. Flow rates in control cells were compared with the rate of flow in the periphery of the kinase-treated cells and the retraction of the central cytoskeleton in cells treated with cytochalasin D (Figure 9A). In cytochalasin D-treated cells the retraction rates were measured by comparing the original cell edge with the outer margin of the central cytoskeleton as well as arcs and membrane discontinuities within this cytoskeleton. Retraction occurred at an essentially constant rate until it stopped (after ~10–40% of the cell radius had been traversed). There was no statistically significant difference between flow rates in control and kinase-treated cells; however, the rate of cytochalasin D-induced retraction was significantly lower than the control cell flow rate. Flow rates were also compared in individual cells before and after treatment with the kinase inhibitors or cytochalasin D. Again there was a significant difference only between rates of flow before treatment and the cytochalasin D retraction.

The drug BDM is a putative low-affinity inhibitor of actomyosin interaction that has been used to test for the involvement of myosin in specific cellular motile events, such as postmitotic cell spreading (Cramer and Mitchison, 1995) and retrograde flow in growth cones (Lin *et al.*, 1996). We used it on coelomocytes to determine what effect it might have on retrograde flow. BDM treatment (15 mM) arrested retrograde flow and disrupted the patterns of actin and myosin II distributions as would be predicted (Figures 10 and 11). However, in contrast to kinase inhibitors, BDM did not produce a medial ridge in treated cells and instead generated the development of a peripheral fringe (Figure 10) via the finite retraction of the cytoskeleton. This retraction was similar to that seen with cytochalasin treatment; however, unlike the cytochalasin-induced actin-free fringe (Figure 7D), the BDM fringe region contained actin filaments, predominantly tangentially oriented, apparently left in the wake of the retracting cytoskeleton (Figure 10, C and D). Thus, the results with BDM were complex, perhaps reflecting the nonspecificity of this inhibitor with regard to actomyosin function.

It is important to point out that retrograde flow was reestablished in subtype 1 coelomocytes when they were washed out of all of the aforementioned drug treatments (cytochalasin D, staurosporine, KT5926, and BDM), suggesting that none of these treatments exerted its effects by simply poisoning the cells. During the washout periods, new flow began at the cell edge and proceeded into the central cytoplasm, "pushing" the existing actin cytoskeleton inward. Eventually the cell recovered to the control pretreatment retrograde flow pattern and cytoskeletal organization. Figure 11 shows a recovery time series of coelomocytes washed

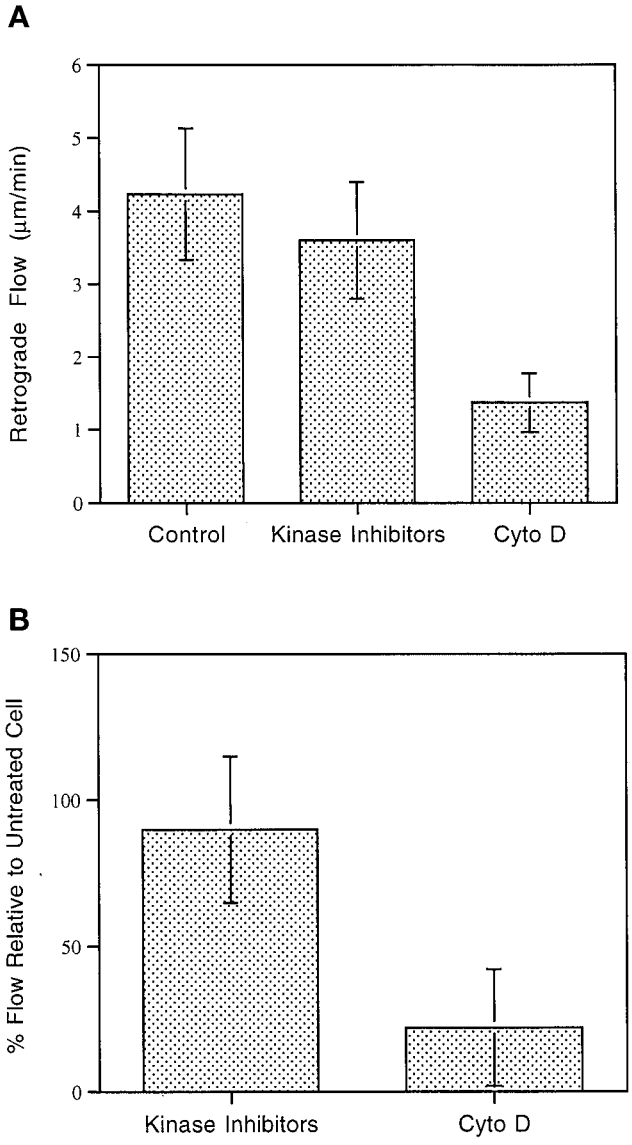

Figure 9. (A) Retrograde flow rate of control cells and cells treated with kinase inhibitors, as well as retrograde retraction of the central cytoskeleton in cells treated with cytochalasin D. Note that the flow rate in control cells is not statistically significantly different from the rate exhibited at the periphery of kinase inhibitor-treated cells; however, it is significantly greater than the cytochalasin D retraction rate ($p = 0.01$). (B) Percent flow in cells treated with kinase inhibitors or cytochalasin D relative to the flow rate in the same cell before treatment.

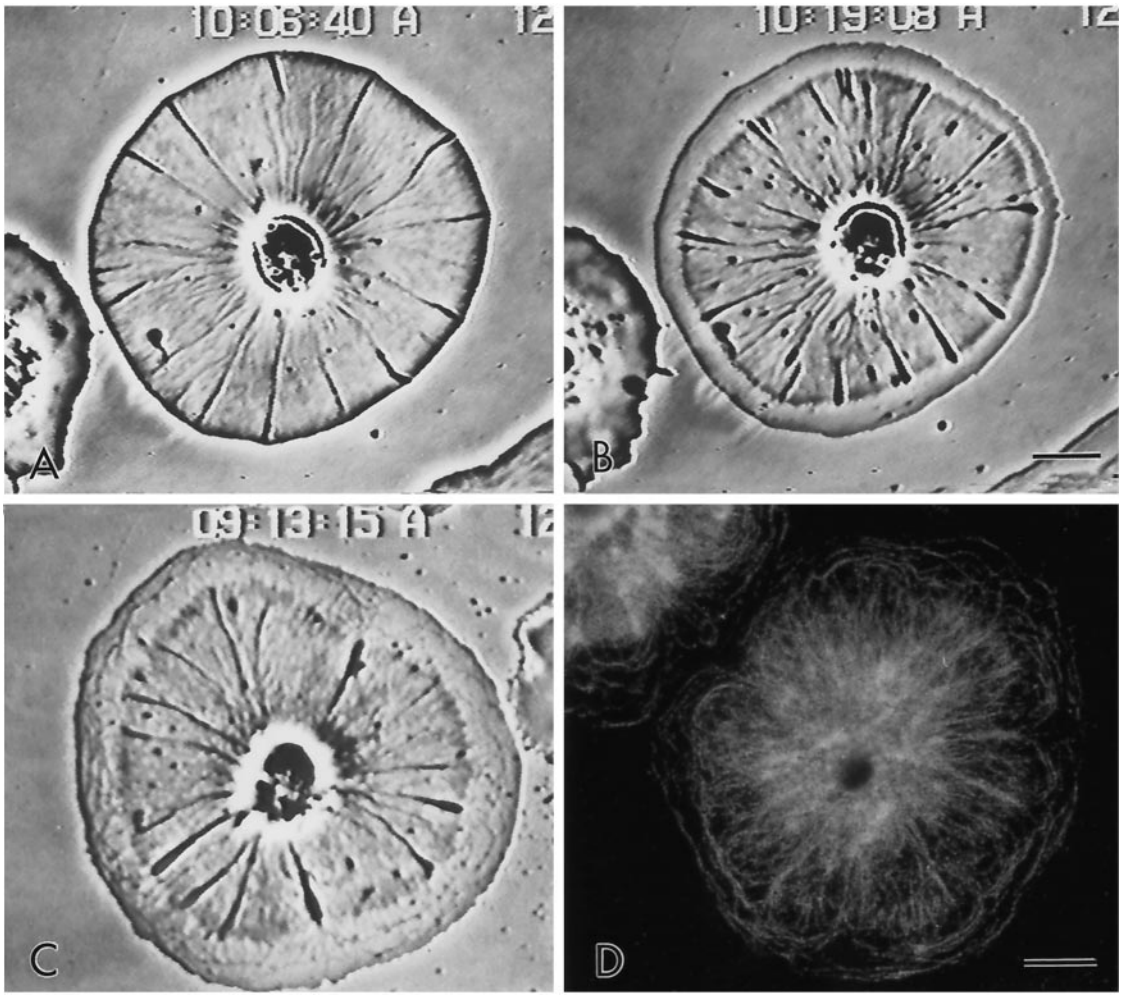

Figure 10. Video-enhanced microscopy of a control subtype 1 coelomocyte (A) and the same cell treated for 5 min with 15 mM BDM (B). The BDM causes the arrest of peripheral flow and development of a cortical fringe through the finite retraction of the central cytoskeleton. The fringe contains tangentially oriented ridges, which become particularly apparent over time (C, cell treated with BDM for 20 min). Rhodamine-phalloidin labeling of actin filaments in a BDM-treated cell (D) demonstrates the tangential actin filaments in the cortical fringe as well as the disrupted nature of the internal actin cytoskeleton. Bar, 10 μm.

out of BDM treatment. Note that the myosin ring is disrupted in cells in which flow is stopped (Figure 11B) and gradually reestablishes itself as flow is restarted (Figure 11, D and F). The results of these washout studies confirm that there is a strong correlation between the occurrence of flow and the existence of a specific actomyosin structure in the cells.

DISCUSSION

Sea urchin coelomocytes offer a unique model experimental system for studying actin-based retrograde and centripetal flow because the nonmotile nature of the cells allows for the flow to be analyzed in the absence of cell translocation. In addition, the extreme flatness and radially symmetric geometry of the cells facilitate microscopic structural analysis. We have exploited these cellular properties to carry out a structural and pharmacological analysis of the retrograde flow mechanism.

Implications from the Structural Organization of the Coelomocyte Cytoskeleton

Our principal structural finding is of the spatial segregation of the myosin II component from the rest of the contractile machinery. In coelomocyte subtype 1 cells, myosin II is organized as a perinuclear network of bipolar filaments and appears to be absent from the rest of the cytoplasm. In contrast, actin filaments are present throughout the cytoplasm, organized as a dense, brush-like network at the cell periphery and more loosely organized radial bundles in the cell interior.

The structural organization of the coelomocyte cytoskeleton immediately suggests a mechanism for the operation of

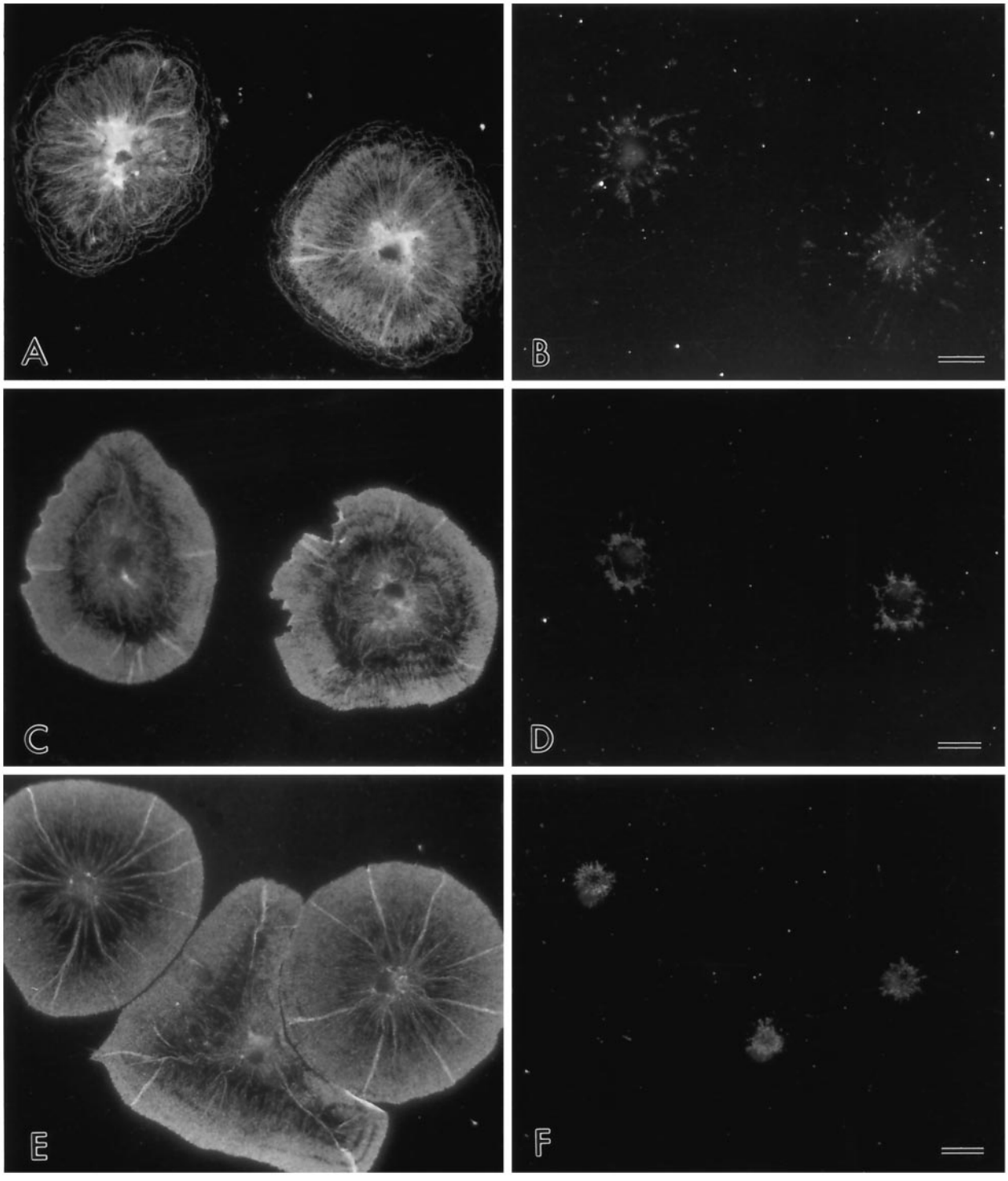

Figure 11. Immunolocalization of actin (A, C, and E) and myosin (B, D, and F) in coelomocytes fixed in the presence of 15 mM BDM (A and B) or after washing out the drug for either 5 min (C and D) or 20 min (E and F). Note that the acto-myosin organizational structure in the cells, which is disrupted by BDM treatment (A and B), gradually reappears during the washout with the reestablishment of retrograde flow (C and D) and by 20 min is essentially identical to that seen in untreated controls (compare E and F with Figure 3, A and B). Bar, 10 μm.

centripetal or retrograde flow. Retrograde flow is visible in the living cells throughout the cytoplasm directed along radial trajectories. Because myosin II is restricted to the cell center, forces exerted locally by myosin II on actin filaments must be transmitted over long distances. For myosin II to be the driver of retrograde flow, the actin filaments with which it is in contact must be interconnected in such a way as to transmit the driving force uniformly through the cytoplasm. The actin network in fact is organized in a suitable manner. The radial bundles extending from the cell center reach all the way to the cell margin. More loosely organized actin filaments also exist between the radial bundles, connecting the bundles with the continuous actin network. Possibly, the partition of actin filaments between loose arrangement and radial bundles reflects tension exerted on them by the myosin II filament network. Finally, actin filaments are organized as a dense, brush-like network at the cell margin. Because the radial bundles connect into this brush-like network, the radially directed tension of the bundles could be diffused by the brush structure and the looser actin network to provide a uniform inward force generating the flow. Thus, the network of myosin II filaments at the cell center may be considered as a "puppeteer" pulling on actin "strings." It is interesting to note that radial actin bundles that exhibit retrograde flow are also present in growth cones and are particularly obvious when imaged using a new polarization microscopy method (Katoh *et al*., 1999).

The actin network structure at the periphery of coelomocytes is similar to that described for keratocytes (Svitkina *et al*., 1997). Recently, the Arp2/3 complex, which has been implicated in actin polymerization (Kelleher *et al*., 1995), has been localized to Y junctions of actin filaments in vitro (Mullins *et al*., 1998) and in vivo (Svitkina and Borisy, 1999), resulting in the proposal of a dendritic nucleation model (Mullins *et al*., 1998) for actin polymerization at the leading edge of motile cells. The branched network structure of actin filaments at the leading edge of coelomocytes may represent another manifestation of dendritic organization. Therefore, the structure of the coelomocyte edge is consistent with its being a major site of actin polymerization, which could help "push" retrograde flow by addition of actin subunits at this site. Together with the localization of myosin II filaments at the cell center, the structural evidence is consistent with a two-component model of retrograde flow.

Implications from Drug-based Function-blocking Experiments

Experiments with agents that inhibit actin polymerization or myosin II function are consistent with both pushing and pulling components. Following previous studies on neuronal growth cones (Forscher and Smith, 1988), we used cytochalasin D to help dissect the retrograde flow mechanism. Cytochalasins bind to the barbed ends of actin filaments and significantly slow actin polymerization rates (Bonder *et al*., 1986). Cytochalasin D treatment of coelomocytes did not block retrograde flow in the cell interior but did lead to the appearance of an actin-free fringe at the periphery as previously reported (Edds, 1993a). Several conclusions may be drawn from this result. Actin polymerization was indeed blocked by cytochalasin D treatment; a mechanism for retrograde flow exists independent of actin polymerization; and the differential behavior of the cell periphery and interior suggest two components to the flow mechanism.

Previous studies on neuronal growth cones (Lin *et al*., 1996) concluded that myosin was the driver for retrograde flow. After this result in neuronal cells, we attempted to block myosin function in coelomocytes with BDM and with protein kinase inhibitors. The BDM experiments were inconclusive, because although the drug did arrest flow, the complexity of the cell's responses to BDM (fringe formation, a finite continuance of interior flow, and a halting of peripheral flow) made the experiments difficult to interpret and suggests a lack of specificity of BDM's action in this system. However, both the broad-spectrum kinase inhibitor staurosporine, and the more myosin light chain kinase-specific inhibitor KT5926 gave interpretable results. Both reagents arrested retrograde flow only in the cell interior and not at the periphery, leading to the formation of a medial ridge, an accumulation of material between the cell edge and cell center. Several conclusions may be drawn from this result, consistent with and complementary to the conclusions from the cytochalasin D experiment. Actin polymerization apparently continued unimpeded by the kinase inhibitors; a kinase inhibitor-sensitive mechanism exists for flow in the interior; and, again, the differential behavior of the cell periphery and interior suggests two components to the flow mechanism. In this respect, it is interesting to note that *Dictyostelium* amoeba lacking myosin II do express centripetal flow, although at much lower rate (Fukui *et al*., 1999). Although other members of the myosin superfamily could conceivably support retrograde flow, our data suggest a possibility that the residual flow in myosin II-null cells may be driven by actin polymerization.

One possible interpretation of the inhibitor experiments, when taken together with the structural data on the spatial segregation of the coelomocyte actin and myosin cytoskeleton, is that pushing by actin polymerization at the periphery represents one component of retrograde flow, and that pulling by myosin II in the interior represents the other. Cytochalasin D, by blocking actin polymerization but not myosin II function, allows pulling to continue in the interior but not for the actin filament population at the periphery to be renewed. Consequently, a clear peripheral fringe develops. The kinase inhibitors, by blocking myosin II function but not actin polymerization, allow pushing to continue at the periphery but not pulling in the interior. Consequently, material accumulates to a medial ridge. Interestingly, the kinase inhibitors also tend to disrupt the radial organization of actin bundles in the interior cytoplasm of the coelomocytes, suggesting that myosin-mediated tension is contributing to the formation of these structures (as theorized by Ingber, 1993; Verkhovsky *et al*., 1999).

Quantitative data on flow rates suggest that the peripheral flow pushing, which persists in cells treated with the kinase inhibitors, is very similar to the flow exhibited by control cells. In contrast, the cytochalasin-induced retraction or pulling rate is slower than flow rates in control cells. It is tempting to speculate that flow rates after drug application reflect the impact of each part of the driving mechanism. Indeed, considering the organization of the coelomocyte cytoskeleton with its elaborated actin-polymerizing machinery at the edge versus the limited myosin assemblages in the center, one might have predicted that, in coelomocytes,

pushing would have a greater impact on flow rate. However, alternative interpretations are also possible.

In the normal situation, pushing and pulling usually operate in tandem, and there is no discernable boundary between their influences. A boundary becomes apparent in cases in which inhibitor treatment has uncoupled the two forces. Sometimes, however, pushing and pulling seem not to be "in pace" with each other even in untreated cells. Thus, ridge-like accumulation of material occasionally appears in some cell sectors (our unpublished observations). Also, light arcs with lower actin contents may arise from a temporarily decreased rate of actin polymerization at the cell edge. We suggest an analogy to a tandem bicycle in which actin pushing and myosin pulling may correspond to the two riders. Both may contribute to the driving force, but, alternatively, one may do most of the work, and other may just keep pace.

Retrograde Flow and Cell Motility

A recent review on cell motility (Heidemann and Buxbaum, 1998) argued for the need for studying actin and myosin II function in the lamellipodia of cells other than keratocytes and neuronal growth cones to evaluate the universality of models of locomotion based on these systems. Retrograde flow has been considered as the action of the locomotory machinery observed "through the looking-glass" (Verkhovsky *et al.*, 1999); in other words, its mechanisms mirror the processes occurring in cellular translocation. From this viewpoint, analysis of retrograde flow in the coelomocyte is relevant to a more general understanding of cell motility.

The crawling motion of animal cells involves three basic steps: formation of a lamellipodial protrusion at the front of the cell, adhesion of the lamellipodium to the substratum, and translocation forward of the cell body. Adhesion of the lamellipodium is necessary for force to produce movement of the cell. An emerging consensus conceptualizes the origin of the cell forces to be of two types. Protrusion at the front is driven by actin polymerization (Condeelis, 1993; Mitchison and Cramer, 1996; Mogilner and Oster, 1996), whereas cell body translocation is driven by myosin II working on the actin network (Cramer and Mitchison, 1995; Svitkina *et al.*, 1997; Verkhovsky *et al.*, 1999). If the cell body were not able to translocate forward either because it was strongly adherent to the substratum or was tethered, the same contractile forces would necessarily result in a retrograde flow. If protrusion could not occur because of opposing membrane tension, the protrusive force of polymerization could also contribute to a retrograde flow. Thus, basic considerations of cell motility suggest the existence of two components of retrograde flow. In the coelomocyte system we interpret the lack of cellular translocation to be a consequence of cell adherence and geometry. The discoidal shape of the cell implies that it may be trying to locomote in all directions simultaneously, and membrane and cytoskeletal constraints prevent it from doing so. In the absence of translocation, the cells exhibit their exaggerated level of retrograde flow. Currently we are attempting to further dissect the mechanisms of flow in coelomocytes through micromanipulation methods aimed at altering cellular geometry and at locally applying cytoskeletal-disrupting drugs.

ACKNOWLEDGMENTS

We are grateful to Robert Mendola for expert technical assistance with coelomocyte TEM sample preparation, David Emlet and Michael Smith for help in the generation of the anti-sea urchin egg myosin antibody, Iain Tomlinson for development of the anti-myosin staining procedures, and Dr. Ralph Cavaleri (Getttysburg College) for help with the use of a Zeiss EM109 TEM. This work was supported by a Whitaker Foundation Student Faculty Research Award from Dickinson College to J.H.H. and R.N., National Science Foundation Young Investigator Award MCB-9257856 and National Institutes of Health grant GM-47693 to J.H.H., and National Institutes of Health grant GM-25062 to G.G.B.

REFERENCES

Anderson, K.I., Wang, Y.L., and Small. J.V. (1996). Coordination of protrusion and translocation of the keratocyte involves rolling of the cell body. J. Cell Biol. *134*, 1209–1218.

Bonder, E.M., and Mosseker, M.S. (1986). Cytochalasin B slows but does not prevent monomer addition to the barbed end of the actin filament. J. Cell Biol. *102*, 282–288.

Bray, D., and White, J.G. (1988). Cortical flow in animal cells. Science *239*, 883–888.

Bryan, J., and Kane, R.E. (1982). Actin gelation in sea urchin egg extracts. Methods Cell Biol. *25*, 175–199.

Cheney, R.E., Riley, M.A., and Mooseker, M.S. (1993). Phylogenetic analysis of the myosin superfamily. Cell Motil. Cytoskeleton *24*, 215–223.

Condeelis, J. (1993). Life at the leading edge: the formation of cell protrusions. Annu. Rev. Cell Biol. *9*, 411–444.

Conrad, P.A., Giuliano, K.A., Fisher, G., Collins, K., Matsudaira, P.T., and Taylor, D.L. (1993). Relative distribution of actin, myosin I, and myosin II during the wound healing response of fibroblasts. J. Cell Biol. *120*, 1381–1392.

Conrad, P.A., Nederlof, M.A., Herman, I.M., and Taylor, D.L. (1989). Correlated distribution of actin, myosin and microtubules at the leading edge of migrating Swiss 3T3 fibroblasts. Cell Motil. Cytoskeleton *14*, 527–543.

Cramer, L.P. (1997). Molecular mechanism of actin-dependent retrograde flow in lamellipodia of motile cells. Front. Biosci. *2*, 260–270.

Cramer, L.P., and Mitchinson, T.J. (1995). Myosin is involved in postmitotic cell spreading. J. Cell Biol. *131*, 179–189.

Cramer, L.P., Siebert, M., and Mitchinson, T.J. (1997). Identification of novel graded polarity actin filament bundles in locomoting heart fibroblasts: implications for the generation of motile force. J. Cell Biol. *136*, 1287–1305.

Debasio, R.L., Wang, L.-L., Fisher, G., and Taylor, D.L. (1988). The dynamic distribution of fluorescent analogues of actin and myosin in protrusions at the leading edge of Swiss 3T3 fibroblasts. J. Cell Biol. *107*, 2631–2645.

Edds, K.T. (1993a). Effects of cytochalasin and colcemid on cortical flow in coelomocytes. Cell Motil. Cytoskeleton *26*, 262–273.

Edds, K.T. (1993b). Cell biology of echinoid ceolomocytes. I. Diversity and characterization of cell types. J. Invert. Pathol. *61*, 173–178.

Fisher, G.W., Conrad, P.A., Debasio, R.L., and Taylor, D.L. (1988). Centripetal transport of cytoplasm, actin and the cell surface in lamellipodia of fibroblasts. Cell Motil. Cytoskeleton *11*, 235–247.

Forscher, P., Lin, C.H., and Thompson, C. (1992). Novel form of growth cone motility involving site-directed actin filament assembly. Nature *357*, 515–518.

Forscher, P., and Smith, S.J. (1988). Actions of cytochalasins on the organization of actin filaments and microtubules in a neuronal growth cone. J. Cell Biol. *107*, 1505–1516.

Fukui, Y., Kitanishi-Yumura, T., and Yumura, S. (1999). Myosin II-independent F-actin flow contributes to cell locomotion in *Dictyostelium*. J. Cell Sci. *112*, 877–886.

Heath, J.P. (1983). Behavior and structure of the leading lamella in moving fibroblasts. I. Occurrence and centripetal movement of arc-shaped microfilament bundles beneath the dorsal cell surface. J. Cell Sci. *60*, 331–354.

Heidemann, S.R., and Buxbaum, R.E. (1998). Cell crawling: first the motor, now the transmission. J. Cell Biol. *141*, 1–4.

Henson, J.H., Nesbitt, D., Wright, B.D., and Scholey, J.S. (1992). Immuolocalization of kinesin in sea urchin coelomocytes: associations of kinesin with intracellular organelles. J. Cell Sci. *103*, 309–320.

Hyatt, H.A., Shure, M.S., and Begg, D.A. (1984). Induction of shape transformation in sea urchin coelomocytes by the calcium ionophore A23187. Cell Motil. *4*, 57–71.

Ingber, D.E. (1993). Cellular tensegrity: defining new roles of biological design that govern the cytoskeleton. J. Cell Sci. *104*, 613–627.

Jay, P.Y., Pham, P.A., Wong, S.A., and Elson, E.L. (1995). A mechanical function of myosin II in cell motility. J. Cell Sci. *108*, 387–393.

Katoh, K., Hammer, K., Smith, P.J.S., and Oldenbourg, R. (1999). Birefringence imaging directly reveals architectural dynamics of filamentous actin in living growth cones. Mol. Biol. Cell *10*, 197–210.

Kazuo, K., Kano, Y., Masuda, M., Onishi, H., and Fujiwara, K. (1998). Isolation and contraction of the stress fiber. Mol. Biol. Cell *9*, 1919–1938.

Kelleher, J.F., Atkinson, S.J., and Pollard, T.D. (1995). Sequences, structural models, and cellular localization of the actin-related proteins Arp2 and Arp3 from *Acanthoamoeba*. J. Cell Biol. *131*, 385–397.

Lee, J., Ishihara, A., Theriot, J.A., and Jacobson, K. (1993). Principles of locomotion for simple-shaped cells. Nature *362*, 167–171.

Lin, C.H., Espreafico, E.M., Mooseker, M.S., and Forscher, P. (1996). Myosin drives retrograde F-actin flow in neuronal growth cones. Neuron *16*, 769–782.

Lin, C.H., and Forscher, P. (1993). Cytoskeletal remodeling during growth cone-target interactions. J. Cell Biol. *121*, 1369–1383.

Lin, C.H., and Forscher, P. (1995). Growth cone advance is inversely proportional to retrograde F-actin flow. Neuron *14*, 763–771.

Mitchinson, T., and Kirschner, M. (1988). Cytoskeletal dynamics and nerve growth. Neuron *1*, 761–772.

Mitchinson, T.J., and Cramer, L.P. (1996). Actin-based cell motility and cell locomotion. Cell *84*, 371–379.

Mogilner, A., and Oster, G. (1996). Cell motility driven by actin polymerization. Biophys. J. *71*, 3030–3045.

Mooseker, M.S., and Cheney, R.E. (1995). Unconventional myosins. Annu. Rev. Cell Biol. *11*, 633–675.

Mullins, R.D., Heuser, J.A., and Pollard, T.D. (1998). The interaction of Arp2/3 complex with actin: nucleation, high affinity pointed end capping, and formation of branching networks of filaments. Proc. Natl. Acad. Sci. USA *95*, 6181–6186.

Nakanishi, S., Yamada, K., Iwahashi, K., Kuroda, K., and Kase, H. (1990). KT5926, a potent and selective inhibitor of myosin light chain kinase. Mol. Pharmacol. *37*, 482–488.

Ostap, E.M., and Pollard, T.P. (1996). Overlapping functions of myosin-I isoforms? J. Cell Biol. *133*, 221–224.

Small, J.V., Herzog, M., and Anderson, K. (1995). Actin filament organization in the fish keratocyte lamellipodium. J. Cell Biol. *129*, 1275–1286.

Smith, S.J. (1988). Neuronal cytomechanics: the actin-based motility of growth cones. Science *242*, 708–715.

Suter, D.M., Errante, L.D., Belotserkovsky, V., and Forscher, P. (1998). The Ig superfamily cell adhesion molecule, apCAM, mediates growth cone steering by substrate-cytoskeletal coupling. J. Cell Biol. *141*, 227–240.

Svitkina, T.M., and Borisy, G.G. (1999). Arp2/3 complex and ADF/cofilin in dendritic organization and treadmilling of actin filament array in lamellipodia. J. Cell Biol. *145*, 1009–1026.

Svitkina, T.M., Surgucheva, I.G., Verkhovsky, A.B., Gelfand, V.I., Moeremans, M., and DeMay, J. (1989). Direct visualization of myosin bipolar filaments in stress fibers of cultured fibroblasts. Cell Motil. Cytoskeleton *12*, 150–156.

Svitkina, T.M., Verkhovsky, A.B., and Borisy, G.G. (1995). Improved procedures for electron microscopic visulatization of the cytoskeleton of cultured cells. J. Struct. Biol. *115*, 290–303.

Svitkina, T.M., Verkhovsky, A.B., McQuade, K.M., and Borisy, G.G. (1997). Analysis of the actin-myosin II system in fish epidermal keratocytes: mechanisms of cell body translocation. J. Cell Biol. *139*, 397–415.

Theriot, J.A., and Mitchinson, T.J. (1991). Actin microfilament dynamics in locomoting cells. Nature *352*, 126–131.

Verkhovsky, A.B., and Borisy, G.G. (1993). Nonsarcomeric mode of myosin II organization in the fibroblast lamellum. J. Cell Biol. *123*, 637–652.

Verkhovsky, A.B., Svitkina, T.M., and Borisy, G.G. (1995). Myosin II filament assemblies in the active lamella of fibroblasts: their morphologies and role in the formation of actin filament bundles. J. Cell Biol. *131*, 989–1002.

Verkhovsky, A.B., Svitkina, T.M., and Borisy, G.G. (1999). Network contraction model for cell translocation and retrograde flow. Biochem. Soc. Symp. *65*, 207–222.

Wang, Y.L. (1985). Exchange of actin subunits at the leading edge of living fibroblasts: possible role of treadmillig. J. Cell Biol. *101*, 597–602.

Wang, Y.L. (1987). Motility of filamentous actin in living cytoplasm. J. Cell Biol. *105*, 2811–2816.

Waterman-Storer, C.M., and Salmon, E.D. (1997). Actomyosin-based retrograde flow of microtubules in the lamella of migrating epithelial cells influences microtubule dynamic instability and turnover and is associated with microtubule breakage and treadmilling. J. Cell Biol. *139*, 417–434.